AMERICAN SOCIETY FOR MICROBIOLOGY | Journal of Bacteriology®

RESEARCH ARTICLE

Orphan Hybrid Histidine Protein Kinase SinK Acts as a Signal Integrator To Fine-Tune Multicellular Behavior in *Myxococcus xanthus*

Maike M. Glaser,[a,b] Penelope I. Higgs[a]

[a]Department of Biological Sciences, Wayne State University, Detroit, Michigan, USA
[b]Department of Ecophysiology, Max Planck Institute for Terrestrial Microbiology, Marburg, Germany

ABSTRACT His-Asp phosphorelay (also known as two-component signal transduction) proteins are the predominant mechanism used in most bacteria to control behavior in response to changing environmental conditions. In addition to systems consisting of a simple two-component system utilizing an isolated histidine kinase/response regulator pair, some bacteria are enriched in histidine kinases that serve as signal integration proteins; these kinases are usually characterized by noncanonical domain architecture, and the responses that they regulate may be difficult to identify. The environmental bacterium *Myxococcus xanthus* is highly enriched in these noncanonical histidine kinases. *M. xanthus* is renowned for a starvation-induced multicellular developmental program in which some cells are induced to aggregate into fruiting bodies and then differentiate into environmentally resistant spores. Here, we characterize the *M. xanthus* orphan hybrid histidine kinase SinK (Mxan_4465), which consists of a histidine kinase transmitter followed by two receiver domains (REC_1 and REC_2). Nonphosphorylatable *sinK* mutants were analyzed under two distinct developmental conditions and using a new high-resolution developmental assay. These assays revealed that SinK autophosphorylation and REC_1 impact the onset of aggregation and/or the mobility of aggregates, while REC_2 impacts sporulation efficiency. SinK activity is controlled by a genus-specific hypothetical protein (SinM; Mxan_4466). We propose that SinK serves to fine-tune fruiting body morphology in response to environmental conditions.

IMPORTANCE Biofilms are multicellular communities of microorganisms that play important roles in host disease or environmental biofouling. Design of preventative strategies to block biofilms depends on understanding the molecular mechanisms used by microorganisms to build them. The production of biofilms in bacteria often involves two-component signal transduction systems in which one protein component (a kinase) detects an environmental signal and, through phosphotransfer, activates a second protein component (a response regulator) to change the transcription of genes necessary to produce a biofilm. We show that an atypical kinase, SinK, modulates several distinct stages of specialized biofilm produced by the environmental bacterium *Myxococcus xanthus*. SinK likely integrates multiple signals to fine-tune biofilm formation in response to distinct environmental conditions.

KEYWORDS *Myxococcus xanthus*, biofilms, development, hybrid histidine kinase

Environmental bacteria are often enriched in signal transduction proteins that allow these organisms to adapt to rapidly changing conditions (1, 2). Proteins that transmit information by histidine-aspartate phosphor transfer, so-called two-component signal transduction proteins, are a common mechanism of signal transduction (3). Genes encoding these proteins can be identified based on conserved signal transmission modules that encode a histidine kinase (HK) domain or a receiver (REC)

Citation Glaser MM, Higgs PI. 2019. Orphan hybrid histidine protein kinase SinK acts as a signal integrator to fine-tune multicellular behavior in *Myxococcus xanthus*. J Bacteriol 201:e00561-18. https://doi.org/10.1128/JB.00561-18.

Editor Ann M. Stock, Rutgers University-Robert Wood Johnson Medical School

Address correspondence to Penelope I. Higgs, pihiggs@wayne.edu.

Received 11 September 2018
Accepted 21 December 2018
Accepted manuscript posted online 7 January 2019
Published 25 February 2019

domain, which accept phosphoryl groups onto invariant histidine or aspartate residues, respectively. Commonly, these domains are found in distinct components, a sensor histidine protein kinase (HPK) that perceives a stimulus, and a response regulator (RR) that mediates a response. In the canonical two-component system, the first component is a membrane-bound HPK that contains a periplasmic sensor domain followed by the cytoplasmic histidine kinase (HK) region (3). Upon stimuli perception by the sensing domain, the HPK autophosphorylates onto an invariant histidine. This phosphoryl group is transferred to an invariant aspartate in an REC domain. Most commonly, REC domains are coupled to an effector domain which mediates a specific response (4). This phosphorylated state promotes a conformational change leading to activation of the effector domain (5). The most common output domain is a DNA binding element, and the RR acts as a transcription factor to regulate gene expression (4). Often, genes encoding the partner HK and RR proteins are adjacent and cotranscribed (6).

A hallmark of this signaling transmitter family is that HK and REC domains are incredibly versatile, and novel signaling systems can easily evolve (7). For instance, sensor histidine kinases may contain multiple sensing domains or lack sensing domains. In addition, some kinases (termed hybrid histidine kinases [HyHKs]) contain one or more REC domains within the same polypeptide (1, 8). HyHKs may participate in His1→Asp1→His2→Asp2 multistep phosphorelay systems, where H2 is from a histidine phosphotransferase domain and D2 is from a terminal response regulator. Alternatively, the HyHK REC domain(s) may serve to modulate kinase activity or kinase output or function as a connector protein to additional kinase proteins (9). These more complex signaling systems play an important, but sometimes hidden, role in integrating and coordinating distinct stimuli for fine-tuned responses.

Myxococcus xanthus is a model organism in which to analyze signaling networks needed to control community behavior (biofilms) in bacteria. These Gram-negative soil bacteria have a life cycle that is facilitated by community behavior (10). Under nutrient-replete conditions, they are cooperative predators; swarms of *M. xanthus* bacteria release antibiotics and degradative enzymes to paralyze, lyse, and digest prey bacteria, fungi, or decaying organic matter. Under nutrient-limited conditions, *M. xanthus* swarms enter a dedicated developmental program during which cells differentiate into the following distinct cell fates: aggregation into haystack-shaped mounds (fruiting bodies) within which cells differentiate into environmentally resistant spores, cell lysis likely via programmed cell death, or formation of a persister-like state (termed peripheral rods) which remain outside the fruiting bodies in a spatially distinct cell fate (11). This developmental program can be considered a specialized version of biofilms produced by the vast majority of bacteria in nature (12). Biofilms are defined as surface-associated communities encased in a self-produced extracellular matrix within which some cells differentiate into resistant (e.g., persister) states (13). Similarly, *M. xanthus* fruiting bodies consist of polysaccharide and extracellular DNA within which cells differentiate into resistant spores (14, 15). *M. xanthus* has advantages as a model system for understanding regulatory mechanisms controlling the production of resistant states in communities, because the sonication-resistant spores are easily quantifiable, and peripheral rods can be easily isolated from the developing population (16).

The *M. xanthus* developmental program is directed by a core genetic regulatory network that is modulated by numerous signal transduction proteins. The 9.2-Mbp *M. xanthus* genome encodes large numbers of phosphohistidine/phosphoaspartate relay proteins, serine/threonine kinases, and proteins involved in secondary messenger signaling (17–21). Furthermore, as observed in particular with the histidine aspartate phosphorelay proteins, many do not appear to follow the canonical "two-component" paradigm of a single HK and RR pair encoded by adjacent genes (18). Of the more than 270 His-Asp phosphorelay proteins encoded in the *M. xanthus* genome, most are genetically orphan (~55%) or located in clusters (~16%) (18, 19), and the cognate partners are difficult to identify. Furthermore, several systems that have been charac-

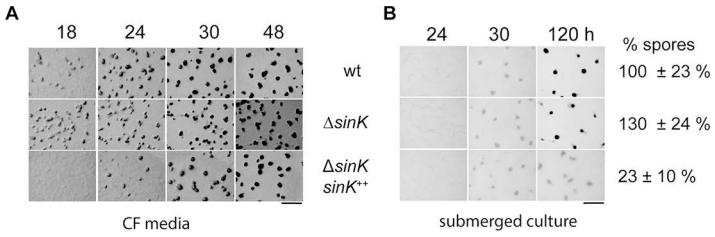

FIG 1 SinK influences aggregation in response to environmental conditions. (A) Developmental phenotype of the DZ2 wild-type (wt) and Δ*sinK* mutant (PH2000), and Δ*sinK* Pr_{pilA}-*sinK* (Δ*sinK sinK*$^{++}$ mutant PH2035) strains induced to develop on CF plates. Ten microliters containing 4×10^8 cells was spotted on each plate, incubated at 32°C, and imaged at the indicated hours of development. (B) Developmental phenotype of the strains indicated in panel A induced to develop under submerged culture. Half a milliliter containing 2×10^7 cells was seeded in one well (24-well plates) and grown for 24 h in rich medium. Development was induced by replacing the medium with starvation buffer. The numbers of heat- and sonication-resistant spores were determined from cells harvested at 120 h of development in submerged culture and recorded as the percentage and associated standard deviation of wild-type spores. Bars = 1 mm.

terized have been demonstrated to have multicomponent and complex phosphorelay proteins (22–26).

In this study, we characterize SinK (signal integrating kinase; Mxan_4465), an orphan hybrid histidine protein kinase consisting of a kinase module followed by two receiver domains. We show that this protein modulates several aspects of the developmental program, including aggregation onset, mobility of aggregates, and sporulation efficiency. Some of these phenotypes were uncovered using a high-resolution submerged-culture developmental assay in which developmental images were recorded in 96-well tissue culture plates every 30 min. Our data suggest that SinK autophosphorylation and/or REC_1 represses aggregation onset depending on the developmental conditions used. Furthermore, SinK autophosphorylation impacts aggregate mobility, and REC_2 impacts sporulation efficiency. SinK appears also to be modulated by a genus-specific hypothetical protein, SinM (signal integration modulator; Mxan_4466). Together, the results of this study provide an additional example of complex signaling systems used to integrate multiple signals to fine-tune behavior.

RESULTS

SinK controls the developmental program in response to environmental conditions. *sinK* is predicted to encode an orphan histidine kinase that was originally identified in a transposon mutagenesis screen designed to identify genes that control developmental progression (K. Cho, P. I. Higgs, and D. Zusman, unpublished data). It was also identified as a histidine kinase that is upregulated during the developmental program (19). To study the role of this kinase further, we generated a *sinK* in-frame deletion (DZ2 Δ*sinK*) and a strain in which this mutant was complemented with *sinK* expressed from the constitutive and highly active *pilA* promoter (27) (Δ*sinK*/*sinK*$^{++}$). We then analyzed the resulting developmental phenotypes compared to the wild-type parent strain, DZ2. When these strains were induced to develop on clone fruiting (CF) nutrient-limited agar, the wild type formed few aggregates by 18 h, the Δ*sinK* mutant strain had already produced numerous aggregation centers by 18 h, and the Δ*sinK*/*sinK*$^{++}$ mutant strain was delayed approximately 6 h (Fig. 1A). These three strains were also analyzed under submerged-culture conditions, wherein vegetative cells growing in a layer on a tissue culture well are induced to develop by replacing rich medium with buffered salts. Interestingly, under submerged culture, both the Δ*sinK* and Δ*sinK*/*sinK*$^{++}$ mutants aggregated with the same apparent timing, i.e., between 24 and 30 h, as the wild type (Fig. 1B). We also measured the efficiency of heat- and sonication-resistant spore production in each mutant at 120 h of development. The wild-type and Δ*sinK* mutant strains produced similar levels of spores, while production in the Δ*sinK*/*sinK*$^{++}$ mutant strain was severely reduced, with approximately 5-fold fewer spores produced after 120 h of development. Thus, native SinK appears to influence the timing of

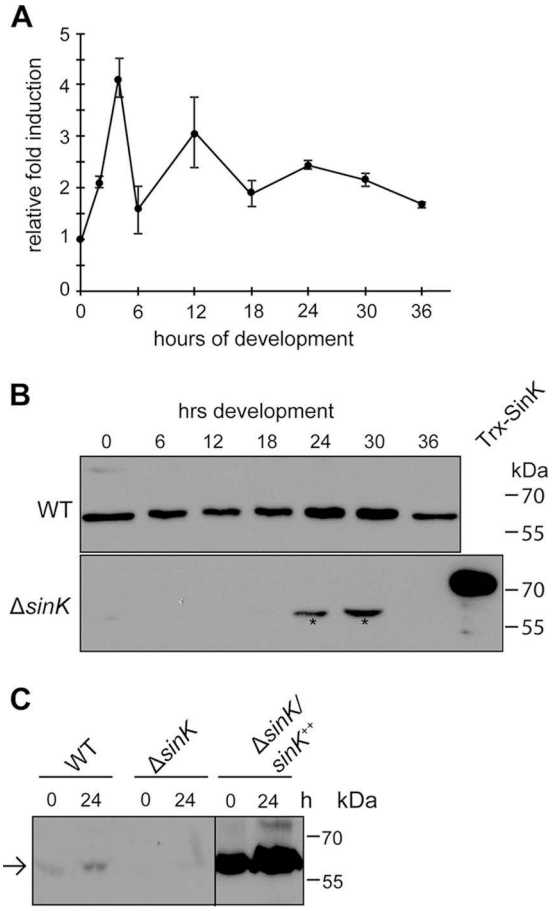

FIG 2 SinK is produced in vegetative and developmental cells. (A) Quantitative real-time PCR analysis of *sinK* mRNA expression. Total RNA isolated from DZ2 wild-type cells at the indicated hours of development under submerged culture was transcribed into cDNA. *sinK* transcripts were detected by real-time PCR. Data points are derived from the average of two experiments. (B) Immunoblot analysis of SinK expression. Protein lysates (10 μg) prepared from wild-type (WT; DZ2) and Δ*sinK* mutant (PH2000) cells developing under submerged culture and harvested at the indicated hours of development were subjected to immunoblotting with anti-SinK polyclonal antisera. *, cross-reactive protein. (C) Anti-SinK immunoblot analysis of wild-type (wt; DZ2), Δ*sinK* mutant (PH2000), and Δ*sinK sinK*$^{++}$ mutant (PH2035) lysates harvested from cells developing 0 and 24 h under submerged culture, as described above.

aggregation in response to different environmental conditions. Furthermore, the observation that overexpression (see below) of SinK reduces sporulation suggests that SinK must either be removed or its signaling state inactivated prior to the onset of sporulation.

SinK is expressed throughout development. To examine the expression profile of *sinK* throughout development, we performed quantitative real-time PCR (qRT-PCR) on cDNA generated from RNA isolated from DZ2 at 0, 2, 4, 6, 12, 24, 30, and 36 h of development under submerged culture. These results indicated *sinK* mRNA was upregulated within 2 h of development, peaked at 4 h (4-fold over time zero [T = 0]), and then decreased to an average of 2-fold over T = 0 after 6 h of development (Fig. 2A). To examine the corresponding protein levels, we generated antibodies specific to SinK and performed a Western blot analysis on cell lysates harvested from the wild-type and Δ*sinK* mutant strains developing under submerged culture. The affinity-purified antiserum detected Trx-His_6-SinK overexpressed and purified from *Escherichia coli* and an ~55-kDa protein (SinK calculated molecular weight, 56.1 kDa) in the wild-type lysate that was absent from most lanes in the Δ*sinK* mutant (Fig. 2B). A similar size band was observed at 24 and 30 h in the Δ*sinK* mutant lysates, which corresponds to a slight increase in signal at those time points in the wild-type lysates; we concluded that a cross-reactive protein comigrates with SinK. Finally, we also confirmed that SinK is

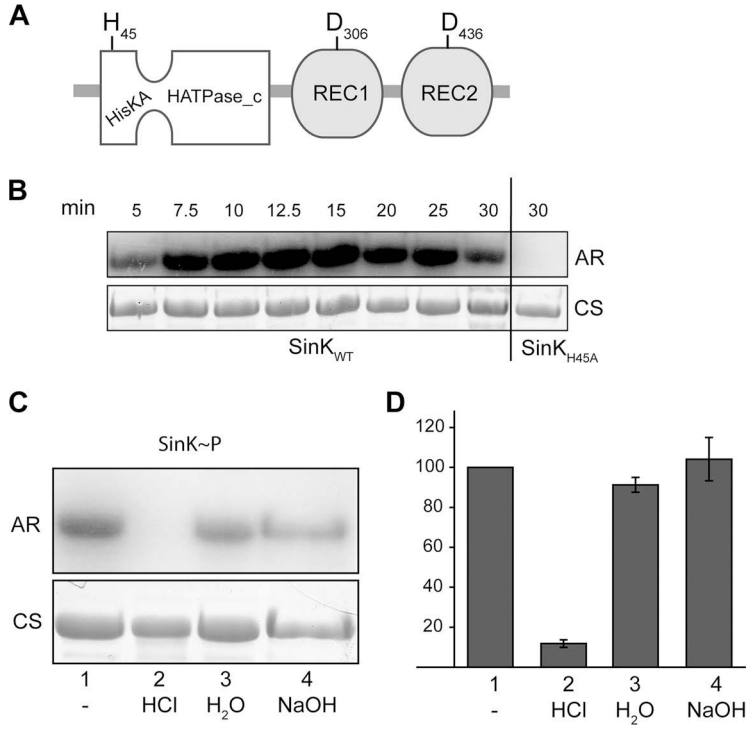

FIG 3 SinK is phosphorylated on histidine residue *in vitro*. (A) Schematic of SinK domain architecture as predicted by SMART analysis (46). Predicted histidine (H) and aspartic acid (D) phosphorylation sites and sequence position are indicated. HisKA, phosphoaccepting and dimerization domain; HATPase_c, ATP hydrolysis domain; REC, phosphoaccepting receiver domain. (B) SinK autophosphorylation assay. Autoradiograph (AR) and corresponding Coomassie blue-stained gel (CS) of 10 μM Trx-His$_6$-SinK or Trx-His$_6$-SinK H45A incubated in the presence of [γ-^{32}P]ATP for the indicated minutes, resolved by SDS-PAGE, and exposed to a phosphoimager screen. (C) Chemical stability of Trx-His$_6$-SinK~P. Trx-His$_6$-SinK~P was autophosphorylated for 30 min as described above, quenched, and denatured, and equivalent aliquots were either frozen immediately or treated with HCl, water, or NaOH for 60 min at 42°C (lanes 1 to 4, respectively). Autoradiography was used for detection as described above. (D) Quantitation of relative band intensities from panel C. Data are the average of the results from four replicates, and error bars display the standard deviation.

highly overproduced in the Δ*sinK*/*sinK*$^{++}$ mutant strain at both 0 and 24 h of development (Fig. 2C). Since SinK was expressed from vegetative cells to at least 36 h (past the onset of sporulation), we concluded that the activity of the SinK protein, rather than its accumulation, is likely necessary to influence aggregation and sporulation.

SinK autophosphorylates *in vitro*. SinK is predicted to be a hybrid histidine kinase containing an N-terminal kinase module and two C-terminal receiver domains (Fig. 3A) (28, 29). To confirm that SinK is a bona fide histidine kinase, we examined whether the protein could autophosphorylate *in vitro*. For these experiments, SinK was overproduced and purified from *E. coli* using N-terminal thioredoxin solubility and hexahistidine affinity tags (Trx-His$_6$-SinK). As a control, we also generated and purified a mutant version of this protein in which the predicted site of autophosphorylation (histidine at position 45) was substituted with an alanine (Trx-His$_6$-SinK$_{H45A}$). When these proteins were incubated in the presence of radiolabeled ATP ([γ-^{32}P]ATP) for 5 to 30 min and then resolved by polyacrylamide gel electrophoresis, incorporation of the radiolabel could be readily detected on Trx-His$_6$-SinK but not Trx-His$_6$-SinK$_{H45A}$ (Fig. 3B and data not shown).

To examine whether autophosphorylated SinK further transferred a phosphoryl group to either of the receivers *in vitro*, we took advantage of the differential chemical stabilities of phosphohistidine (acid labile, base stabile) versus phosphoaspartic acid residues (acid and base labile) (30). For these experiments, we allowed Trx-His$_6$-SinK to autophosphorylate in the presence of [γ-^{32}P]ATP for 30 min, quenched the reaction with protein sample buffer, and then divided the reaction mixture into four aliquots.

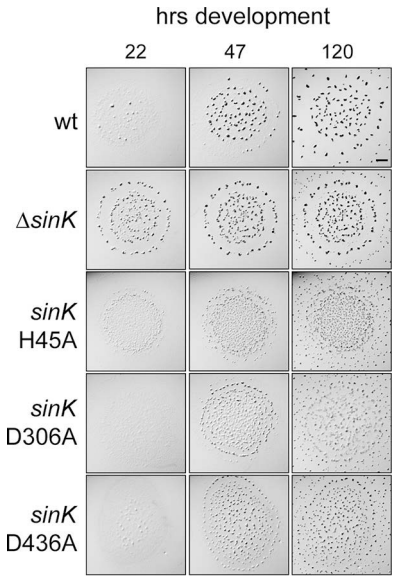

FIG 4 SinK kinase and receiver 1 are necessary for appropriate aggregation on CF developmental medium. Developmental phenotype of wild-type (wt; DZ2), Δ*sinK* mutant (PH2000), $sinK_{H45A}$ mutant (PH2013), $sinK_{D306A}$ mutant (PH2014), or $sinK_{D436A}$ mutant (PH2015) strains induced to develop on CF plates as described for Fig. 1A. Bar = 1 mm.

One aliquot was immediately placed at −20°C (control reaction), and the remaining three aliquots were additionally incubated in the presence of water, 1 M HCl, or 1 M NaOH for 60 min at 42°C. Equivalent proportions of all four reaction mixtures were then resolved by SDS-PAGE, and radiolabel incorporation retained on the protein was examined and quantitated (Fig. 3C and D). Relative to the control reaction, treatment with HCl caused a loss of more than 88% of the signal. In contrast, treatment with water or NaOH did not significantly affect the amount of radiolabel associated with Trx-His_6-SinK. Together, these results suggested that the protein was phosphorylated solely on H_{45}, and phosphotransfer to either REC domain was not observed *in vitro*.

SinK autophosphorylation is necessary to repress aggregation on CF. We next set out to examine whether SinK autophosphorylation or receiver domain phosphorylation was necessary for protein function *in vivo* by generating a substitution of the invariant histidine or aspartic acid residues which are predicted to be phosphorylated in each domain. To examine whether kinase activity is needed, we substituted the histidine at position 45 with an alanine ($sinK_{H45A}$) in the endogenous locus. When cells were induced to develop on CF plates, the $sinK_{H45A}$ mutant began to aggregate about 6 h earlier than the wild type, but it produced smaller and more numerous aggregates than did the wild-type or Δ*sinK* mutant cells (Fig. 4). To next examine whether phosphorylation of the first receiver (REC_1) or second receiver (REC_2) domains were important for SinK function *in vivo*, we generated mutations in the endogenous *sinK* locus in which the predicted phosphoaccepting aspartate codon at amino acid 306 (D_{306}) or 436 (D_{436}) was substituted with an alanine codon ($sinK_{D306A}$ or $sinK_{D436A}$, respectively) (Fig. 4). When these mutants were analyzed on CF, the $sinK_{D306A}$ strain appeared to be very slightly delayed relative to the wild type, while development of the $sinK_{D436A}$ strain appeared indistinguishable from that of the wild type. These *sinK* point mutations did not appear to negatively impact SinK stability, because similar levels of SinK could be detected between each mutant and the wild type, as assayed by anti-SinK immunoblot analysis of lysates generated from developing cells (see Fig. S1 in the supplemental material).

A high-resolution submerged-culture developmental assay reveals that SinK autophosphorylation impacts aggregate mobility, and SinK REC_1 phosphorylation likely impacts aggregation onset. Although our submerged-culture developmental

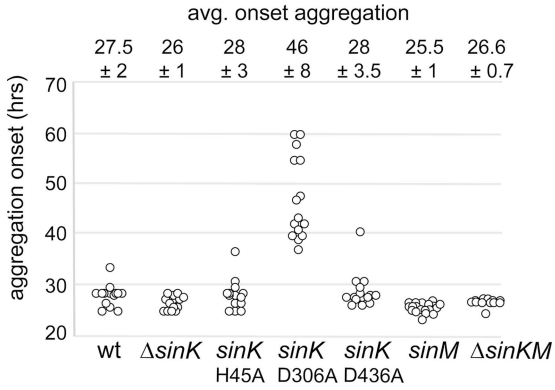

FIG 5 Summary of *sinK* mutant developmental phenotypes under high-resolution submerged culture. Analysis of aggregation onset using high-resolution submerged-culture assays. A volume of 0.15 ml containing 2×10^7 cells of wild-type (wt; DZ2), Δ*sinK* mutant (PH2000), $sinK_{H45A}$ mutant (PH2013), $sinK_{D306A}$ mutant (PH2014), $sinK_{D436A}$ mutant (PH2015), *sinM* insertion mutant (*sinM*::pMG011; PH2018), and Δ(*sinKM*) mutant (PH2009) strains was seeded in one well (96-well microtiter plates) and grown for 24 h in rich medium. Development was induced by replacing the medium with starvation buffer. Cells were imaged every 30 min from 24 to 72 h of development. Data are summarized from three independent biological replicates each containing five technical replicates. The first frame in which aggregates could be identified was used to calculate the aggregation onset for each movie. Average (avg.) time and associated standard deviation of aggregation onset are displayed above the relevant mutants.

analyses suggested that *sinK* mutants did not display an obvious aggregation phenotype (Fig. 1B and data not shown), we speculated that the timing and mobility of the aggregates may have been overlooked in these static assays. To gain further resolution of the aggregation phenotypes for all the *sinK* mutants, we designed a high-resolution submerged-culture developmental assay in which cells were seeded into 96-well tissue culture plates. After 24 h of starvation, each well was imaged every 30 min for the next 48 h in an automated plate reader. Images were compiled to monitor the progression of development in each strain (representative Movies S1 to S5). Using this method, we could detect differences in the onset of aggregation with a resolution of 30 min. Analysis of 15 total movies from each strain (five technical replicates from each of three independent biological replicates) indicated that the wild-type strain began to aggregate at 27.5 ± 2 h of development (Fig. 5). The onset of aggregation times in the Δ*sinK*, $sinK_{H45A}$, and $sinK_{D436A}$ mutants were not significantly different from that in the wild type (26 ± 1, 28 ± 3, and 28 ± 3.5 h development, respectively). In contrast, the $sinK_{D306A}$ mutant showed a strongly delayed onset of aggregation (46 ± 8 h development) (Fig. 5).

We also quantified other characteristics of aggregate formation, including maximum observed initial aggregates and final number of fruiting bodies at 72 h of development (Fig. 6A), as well as relative mobility of aggregates (Fig. 6B). These analyses revealed that the wild-type strain initially produced 3 to 14 aggregates that either dissolved or coalesced to much fewer (3 to 6) fruiting bodies (Fig. 6A). These aggregates were mobile for 21 ± 12 h (Fig. 6B). The Δ*sinK* and $sinK_{H45A}$ mutants produced a similar number of aggregates as the wild type (from 4 to 14 and 4 to 13 aggregates, respectively), but ultimately, most of these aggregates produced mature fruiting bodies (4 to 12 and 4 to 14, respectively) (Fig. 6). Correspondingly, the aggregates produced by these mutants were mobile for only 11 ± 7 and 0 ± 0 h, respectively (Fig. 6). The $sinK_{D436A}$ mutant produced a wide range of aggregates (1 to 18) that matured into a similar range of fruiting bodies (1 to 15); these aggregates displayed no mobility (0 ± 0 h). The $sinK_{D306A}$ mutant mostly produced fewer aggregates (1 to 10) that failed to mature in the time frame measured (Fig. 6); we did not calculate the average aggregate mobility because aggregates were still moving by the final frame recorded. Together, these results suggested that SinK REC_1 phosphorylation is necessary to efficiently induce aggregation, whereas SinK autophosphorylation and REC_2 phosphorylation played a role in transition into immobile fruiting bodies.

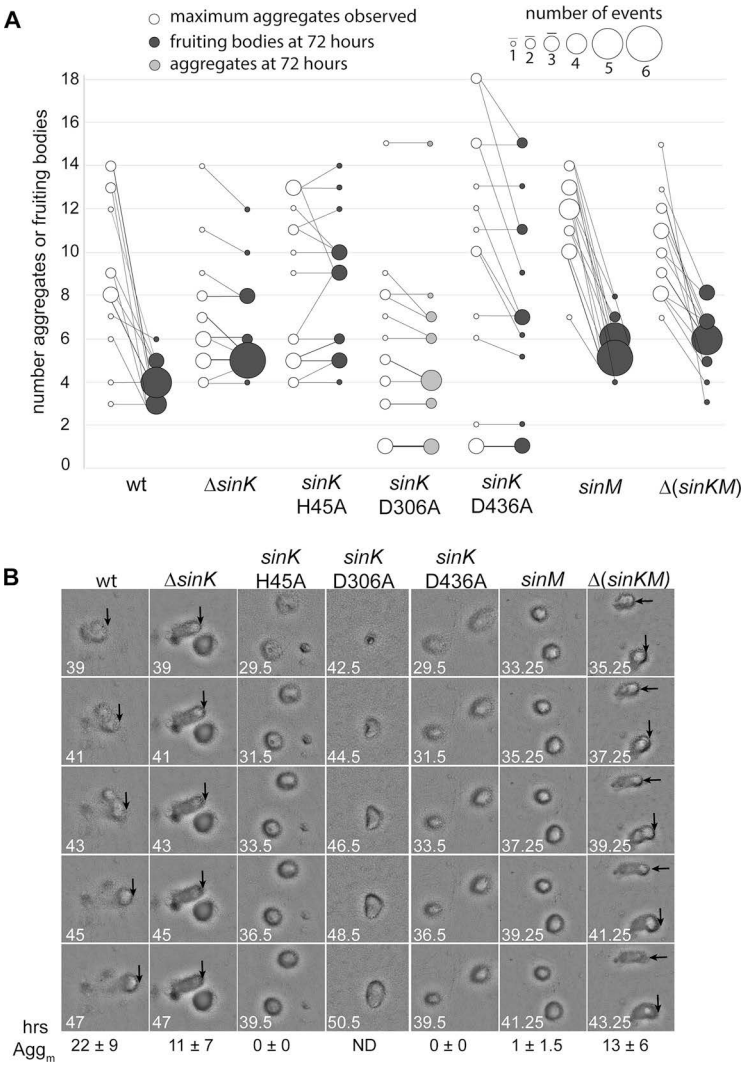

FIG 6 SinK mutants display reduced aggregate mobility. (A) Analysis of the maximum number of initial aggregates (white circles) and the final number of stationary fruiting bodies (black circles) observed with wild-type (wt; DZ2), Δ*sinK* mutant (PH2000), $sinK_{H45A}$ mutant (PH2013), $sinK_{D306A}$ mutant (PH2014), $sinK_{D436A}$ mutant (PH2015), *sinM* insertion mutant (*sinM*::pMG011; PH2018), and Δ(*sinKM*) mutant (PH2009) strains developed by high-resolution submerged culture (as for Fig. 5). Gray circles represent immature aggregates observed at 72 h of development. The diameter of the circles corresponds to the incidence of a given number of aggregates or fruiting bodies observed, as indicated by the legend. Lines connect the number of maximum aggregates and final fruiting bodies observed in a given well. (B) Representative relative mobility of aggregates observed by the strains in panel A. Equivalent areas of individual frames are displayed from the hours of development indicated in the frame corners. Arrows denote the leading edge of mobile aggregates. Average hours of aggregate mobility and associated standard deviation are indicated below the last frame. ND, not determined.

SinK REC_2 phosphorylation is likely necessary for appropriate sporulation. Analysis of the *sinK* mutants under a high-resolution submerged-culture assay suggested that these mutants transitioned from mobile aggregates to stationary fruiting bodies more rapidly than did the wild type. We hypothesized that aggregate mobility could be affected by the onset of sporulation because spores are clearly nonmotile. We therefore next examined the rate at which spores were produced in each of these mutants when they were developed under submerged culture for 48, 72, or 120 h of starvation. The wild type produced 1.7 ($\pm$1.4) $\times$ 10^6 spores per well at 48 h development, which increased to 1.7 ($\pm$0.4) $\times$ 10^7 spores by 120 h of development (Fig. 7). The Δ*sinK* mutant produced spores at a rate which was not significantly different from that of the wild type. Interestingly, the $sinK_{H45A}$ mutant produced more spores than did the wild type

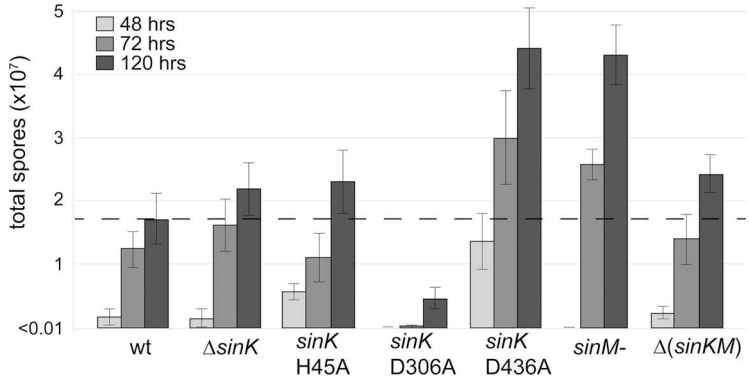

FIG 7 SinK receiver 2 and SinM are necessary for appropriate sporulation. Numbers of heat- and sonication-resistant spores produced at the indicated time from wild-type (wt; DZ2), Δ*sinK* mutant (PH2000), $sinK_{H45A}$ mutant (PH2013), $sinK_{D306A}$ mutant (PH2014), $sinK_{D436A}$ mutant (PH2015), *sinM* insertion mutant (*sinM*::pMG011; PH2018), and Δ(*sinKM*) mutant (PH2009) strains induced to develop under submerged culture in 24-well tissue culture plates are shown, as described for Fig. 1. Data are presented as average and associated standard deviation of the results from triplicate replicates. Similar trends were observed in two independent biological replicates.

by 48 h, but by 72 and 120 h, the number of spores was not significantly different from that of the wild type. Analysis of the $sinK_{D306A}$ mutant indicated that sporulation was strongly delayed and reduced, consistent with the delay in aggregation observed in this mutant. Surprisingly, spore production in $sinK_{D436A}$ mutant cells was at least 2-fold increased at each time point, ultimately producing ~3-fold more spores than the wild type at the completion of development. Together, these results suggested that SinK REC_2 phosphorylation might delay sporulation, thus increasing the time period of aggregate mobility. The different roles of kinase autophosphorylation and REC_1 and REC_2 phosphorylation suggested an unusual method of signaling control in this protein.

***sinK* is cotranscribed with a gene encoding a hypothetical protein that is specific to the *Myxococcales*.** SinK is an unusual signal transduction protein for which both an obvious sensor domain and output domain are lacking (Fig. 3A). In attempt to identify additional components that may activate or serve as effectors for SinK activity, we turned to genes near *sinK*. Analysis of the genetic locus suggested that the stop codon predicted for *sinK* overlaps a predicted start codon for the adjacent downstream gene, *sinM* (Mxan_4466) (Fig. S2A). To determine whether *sinK* and *sinM* are cotranscribed, we isolated DNA-free RNA from wild-type cells induced to develop for 3 h and reverse transcribed it into cDNA using a reverse primer specific to a region starting 247 bp downstream from the predicted *sinM* start codon. When this cDNA reaction was used as the template in a PCR, we could amplify two regions spanning the 3′ end of *sinK* and the start of *sinM*, bp −53 to +145 of *sinM* and bp −177 to +145 (Fig. S2A, regions 2/3 and 5/3, respectively, and B). We could also amplify bp 1195 to 1338 of *sinK* (Fig. S2A, regions 4 to 6, and B). Identical amplicons were detected if genomic DNA was used as the template. Amplicons were not detected using control cDNA reactions in which the reverse transcriptase was omitted (Fig. S2B). Thus, *sinK* and *sinM* are transcribed into the same polycistronic mRNA. Because the genes flanking *sinK* and *sinM* are predicted to be transcribed from the opposite direction, the operon likely consists solely of these two genes.

To begin to understand the function of SinM, we next subjected the protein sequence to bioinformatic analyses. pBLAST analysis indicated that no characterized functional domains could be identified, and SinM was annotated as a hypothetical protein with homologs (E value $< 10^{-10}$) only within the *Myxococcus* genus (Fig. S4). In the species where *sinM* homologs were detected, synteny was conserved with *sinM* located between *sinK* and a *groEL* homolog (Fig. S4). In myxobacterial species that lacked *sinM* homologs, *sinK* was located adjacent to the *groEL* homolog. Together, these

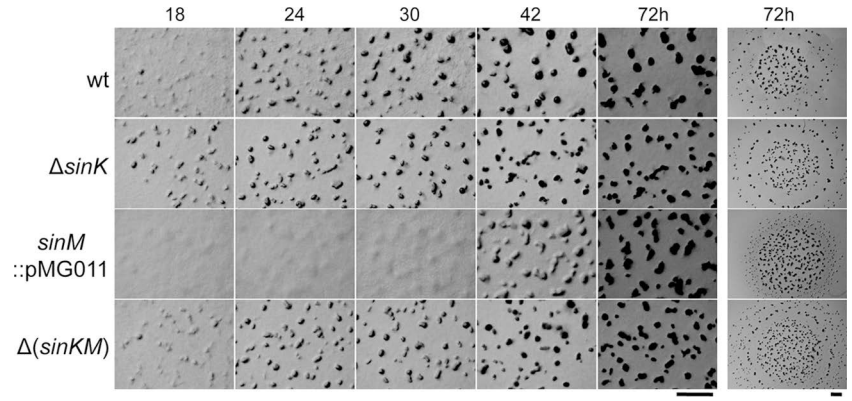

FIG 8 Genetic analysis suggests that *sinM* encodes a protein necessary to stimulate aggregation through SinK. Developmental phenotype of wild-type (wt; DZ2), Δ*sinK* mutant (PH2000), *sinM* insertion mutant (*sinM*::pMG011; PH2018), or Δ(*sinKM*) mutant (PH2009) strains induced to develop on CF plates, as described for Fig. 1A. The Δ*sinK* phenotype is epistatic to the *sinM* phenotype. Bars = 1 mm.

data suggested that SinM was likely involved in modulating SinK activity in a process that was restricted to *Myxococcus* species. We next investigated the phenotype of a *sinM* disruption mutant as a first step to determine whether they may function together.

SinM acts through SinK to control aggregation and/or sporulation. To examine whether SinM also plays a role in the regulation of development, we generated an insertion mutant in which *sinM* was disrupted after codon 221. When this mutant was analyzed for development on CF plates, aggregation was not observed until approximately 24 h later than for the wild type (Fig. 8). We were unable to generate an in-frame deletion of *sinM*. As an alternate approach, we converted the TGC codon at position 15 to a TGA stop codon via a cytosine-to-adenine substitution ($sinM_{stop}$). This mutant produced a strongly delayed developmental phenotype similar to that produced by the *sinM* disruption (Fig. S3). As the Δ*sinK* and *sinM* mutants displayed opposing phenotypes, we next examined the CF developmental phenotype of a mutant in which the entire *sinKM* locus was deleted. This Δ(*sinKM*) mutant phenocopied the Δ*sinK* mutant, in that cells began to aggregate at least 6 h earlier than in the wild type (Fig. 8).

Further analysis of the *sinM* and Δ(*sinKM*) mutants by high-resolution submerged-culture assay indicated that the onset of aggregation was 25.5 ± 1 and 26.6 ± 0.7 h, respectively, which was indistinguishable from all mutants except that of the strongly delayed $sinK_{D306A}$ (Fig. 5 and Movies S6 and S7). Only subtle differences were observed in the maximum aggregates and mature fruiting bodies produced by *sinM* and Δ(*sinKM*) mutants (Fig. 6A). Strikingly though, the *sinM* aggregates were essentially immobile (aggregate mobility [Agg_m], 1 ± 1.5 h), while the Δ(*sinKM*) mutant aggregate mobility was similar to that of the Δ*sinK* mutant (Agg_m, 13 ± 6 and 11 ± 7 h, respectively) (Fig. 6B). Finally, the *sinM* mutant displayed enhanced sporulation at 72 and 120 h of development (>2-fold higher than that of the wild type and similar to levels observed in the $sinK_{D436A}$ mutant) (Fig. 7). In contrast, the Δ(*sinKM*) mutant sporulation efficiency was similar to that of the Δ*sinK* mutant (Fig. 7). Together, these data suggest that (i) the *sinK* phenotype is epistatic to that of *sinM*, suggesting that SinM functions via modulation of SinK activity, (ii) SinM induces aggregation on CF medium likely by antagonizing phosphorylated SinK (SinK~P), and (iii) SinM increases aggregate mobility and reduces sporulation efficiency likely via modulation of SinK REC_2 phosphorylation.

DISCUSSION

In this study, we characterized an unusual hybrid histidine protein kinase, SinK, which consists entirely of His-Asp phosphorelay signal transmission domains: an amino-terminal kinase domain followed by two receiver domains (Fig. 3A). We could show that SinK readily autophosphorylated *in vitro*, but we did not detect phosphotransfer to its

two associated REC domains (Fig. 3B and C). Genetic evidence strongly suggested that phosphorylation of the REC domains is important *in vivo*, and that SinK kinase autophosphorylation is likely not the phosphodonor (discussed below). Instead, we propose that one or more unknown protein kinases likely phosphorylate the SinK receiver domains in a process which can be modulated by the hypothetical protein SinM. Using a newly developed high-resolution submerged-culture assay, we observed that SinKM appeared to act together on several distinct stages in *M. xanthus* development, as follows: aggregate onset, dissolution of aggregates and/or aggregate mobility, and sporulation efficiency.

Although not definitive, a possible model for how SinKM could function is outlined here. Under submerged-culture development, SinK REC_1 must be phosphorylated to allow appropriate aggregation onset, because the unphosphorylated state of SinK REC_1 actively prevents aggregation onset, perhaps by preventing the accumulation of protein necessary to stimulate aggregation. This aspect is supported by the observation that the $sinK_{D306A}$ mutant is strongly delayed in aggregation, but if the entire protein is absent (Δ*sinK* mutant), normal aggregation onset is observed (Fig. 5). We propose that SinK REC_1 is phosphorylated by an unknown kinase activated under submerged-culture conditions, because the $sinK_{H45A}$ mutant is not likewise delayed. After the formation of aggregation centers, SinK can be stimulated to autophosphorylate, which then delays the transition to stationary fruiting bodies, because the $sinK_{H45A}$ mutant produces stationary aggregates that rarely dissolve or travel (Fig. 6). During this period, we propose that SinM may antagonize SinK autophosphorylation and promote SinK REC_2 phosphorylation to promote aggregate mobility and delay sporulation onset and efficiency, because both the $sinK_{D436A}$ and *sinM* mutants display reduced aggregate mobility and sporulate more efficiently than the wild type (Fig. 7). Again, the SinK kinase domain is likely not the sole phosphodonor for REC_2 because the $sinK_{H45A}$ mutant displays wild-type sporulation levels. It is likely that the phosphorylation state of the kinase domain or either receiver domain influences the activity of the others, which would serve to coordinate the activities regulated by each domain. This possibility could be supported by analysis of developmental phenotypes displayed by double point mutants (e.g., $sinK_{D306A\ D436A}$), but for unknown reasons, we were unable to recover this (or any other combination) double substitution in *sinK*.

Our data also suggest that SinK autophosphorylation and SinM activity are influenced differently when cells are induced to develop on CF agar. Under CF conditions, the $sinK_{H45A}$ and Δ*sinK* mutants began to produce aggregation centers earlier than did the wild type (Fig. 4), while the *sinM* mutant was strongly delayed (Fig. 8). These data suggested that SinK autophosphorylates when cells are in the preaggregation stage to repress aggregation onset. In addition, SinM appears to antagonize SinK autophosphorylation. The nature of the stimuli that influence SinK and SinM in the preaggregation stage under CF (but not submerged-culture) conditions is not known, but differences in the two developmental conditions involve nutrient levels, substratum surface, differences in oxygen availability, and number of cells. We ruled out cell number, because induction of development with a range of cell densities did not alter the relative difference in aggregation onset between the Δ*sinK* mutant and wild-type strains (our unpublished data). SinM is likely responding to inputs to modulate SinK domains, but there is little clue as to its exact function. SinM is annotated as a hypothetical protein that contains a domain of unknown function (DUF5050). The gene is so far only identified in the *Myxococcus* genus, although *sinK* is found throughout the *Cystobacteraceae* (see Fig. S4 in the supplemental material). Thus, *sinM* appears to be a recently acquired gene, and its modulation of SinK function may be an example of niche-specific adaptation.

It is also unknown how SinK may be influencing the different aspects of the developmental program. One possibility is that SinK targets a core developmental protein that plays a role in both aggregation and sporulation, such as the global transcriptional regulator MrpC (31, 32). Consistently, our initial analyses suggested that MrpC protein accumulates early in the Δ*sinK* mutant and is repressed in the Δ*sinK*/

sinK^{++} mutant strain (our unpublished data). We are currently further exploring this hypothesis.

What advantage does this complex signaling system provide for *M. xanthus*? The observed differences in phenotype depending on developmental conditions suggest that SinKM may serve to adapt fruiting bodies to specific environmental conditions. It is tempting to speculate that in wild-type cells, aggregate mobility allows groups of cells to optimize fruiting body size or to make one last attempt to explore the environment before committing the group to sporulation. Perhaps producing larger, coalesced fruiting bodies (via stimulation of SinK autophosphorylation) provides a fitness advantage, because they provide greater protection from environmental insults and/or facilitate dispersal of larger groups of cells to new environments to allow germination into more productive feeding colonies. However, in certain environments, it may be more advantageous to quickly produce fruiting bodies (via decreasing phosphorylated REC_2 [REC_2~P]). Alternatively, by launching sporulation earlier, more energy resources are available for the production of resistant spores, such as the expensive production of the spore coat (33).

Although the model of SinKM function seems unusually complex, it belongs to an increasing list of characterized multidomain and/or multicomponent signaling proteins that appear to coordinate aspects of the *M. xanthus* developmental program. Examples include the RodK/RokA system, consisting of a triple receiver hybrid histidine kinase and single-domain response regulator that influence appropriate localization of spores within fruiting bodies (22, 34); the EspA/EspC system, hybrid histidine kinases that cross-phosphorylate to regulate appropriate timing and spore location via turnover of the major transcription factor MrpC (25, 35); the RedCDEF four-component system necessary for appropriate aggregation timing (23); the CrdA/S system necessary for appropriate developmental entry (24); the PilSR/S_2R_2 system necessary for coordinated type 4 pilus regulation (26); and the FrzE/FrzZ/FrzX system that serves to coordinate cell reversals necessary for *M. xanthus*-directed movement (36). These complex integrated strategies appear to be common in environmental bacteria and likely allow for integrated responses to rapidly changing environmental conditions (37).

MATERIALS AND METHODS

Bacterial strains and growth conditions. The bacterial strains and plasmids used in this study are listed in Table 1. *Escherichia coli* strains were grown under standard laboratory conditions in LB medium and supplemented with 50 μg ml^{-1} kanamycin and/or 100 μg ml^{-1} ampicillin where necessary (38). *M. xanthus* strains were grown under vegetative conditions in Casamino Acids-yeast extract (CYE) broth (with shaking at 250 rpm) or on CYE-1.5% agar plates (39) at 32°C and supplemented with 100 μg ml^{-1} kanamycin where necessary.

Construction of plasmids and strains. The plasmids and primers used in this study are listed in Table S1 in the supplemental material. Plasmids used to generate in-frame deletions or point mutations were constructed by using overlap PCR with the indicated primers. The overlap PCR protocol is described in detail elsewhere (40). The fused PCR product was cloned into the indicated sites of pBJ114. All plasmid inserts were sequenced to confirm the absence of PCR-generated errors, and point mutations in the *M. xanthus* genome were confirmed by sequencing PCR products amplified from the mutant genome.

Strains bearing in-frame deletions or point mutations in endogenous loci were generated using the plasmids indicated in Table S1 and the kanamycin-resistant/*galK*-positive/negative-selection strategy (41), as described in detail previously (40). Strains bearing plasmids integrated at the genomic *attB* site were generated by site-specific recombination with plasmids bearing the Mx8 phage *attP* site (42); integration was selected by plasmid-borne resistance to kanamycin at 100 μg ml^{-1}. Proper integration was confirmed by PCR, as per Magrini et al. (42). Strains were then single colony purified to ensure pure mutant cultures.

Developmental assays. Development of *M. xanthus* strains on CF plates was performed as described previously (40). Briefly, vegetative cells were harvested from broth culture, washed with MMC salts (10 mM morpholinepropanesulfonic acid [MOPS] [pH 7.6], 4 mM $MgSO_4$, 2 mM $CaCl_2$), and resuspended to an absorbance at 550 nm (A_{550}) of 7 in MMC, and 10-μl spots were applied to CF plates (39). Development under submerged culture was performed as described previously (40). Briefly, cells were grown overnight in CYE broth and diluted to an A_{550} of 0.035 in fresh CYE medium, and then 16.0 ml, 0.5 ml, or 0.15 ml was seeded into 100-mm petri dishes, one well of a 24-well plate, or one well of a 96-well plate, respectively. Cells were grown into a confluent layer for an additional 24 h at 32°C. To initiate the developmental program, CYE was replaced by an equivalent volume of MMC, followed by continued incubation at 32°C. Pictures were recorded with a Leica M80 stereomicroscope at the times of development indicated in each figure.

TABLE 1 Strains and plasmids used in this work

Strain or plasmid	Genotype or description[a]	Source or reference
Strains		
M. xanthus		
DZ2	Wild type	39
PH2000	DZ2 Δ*sinK*	This study
PH2035	PH2000 *attB*::pMG017 (Pr_{pil}-*sinK*) Km^r	This study
PH2013	DZ2 $sinK_{H45A}$	This study
PH2024	DZ2 $sinK_{D306A}$	This study
PH2015	DZ2 $sinK_{D436A}$	This study
PH2018	DZ2 *sinM*::pMG011 Km^r	This study
PH2016	DZ2 $sinM_{stop}$	This study
PH2009	DZ2 Δ(*sinKM*)	This study
E. coli		
TOP10	F^- *endA1 recA1 galE15 galK16 nupG rpsL ΔlacX74 ϕ80lacZ*ΔM15 *araD139* Δ(*ara leu*)*7697 mcrA* Δ(*mrr-hsdRMS-mcrBC*) λ^-	Invitrogen
GJ1158	F^- *ompT gal dcm lon* $hsdS_B(r_B^-\ m_B^-)$ proUp::T7 RNAP	45
Plasmids		
pBJ1114	*galK* Km^r	47
pSWU30	Mx8 *attP* Km^r	48
pΔMXAN4465	pBJ114 Δ*sinK* Km^r	19
pMG017	pSL8 Pr_{pilA}-*sinK* Km^r	This study
pMG008	pBJ114 $sinK_{H45A}$ Km^r	This study
pMG009	pBJ114 $sinK_{D306A}$ Km^r	This study
pMG010	pBJ114 $sinK_{D436A}$ Km^r	This study
pMG011	pBJ114 Δ*sinM* Km^r	This study
pMG012	pBJ114 $sinM_{stop}$ Km^r	This study
pMG004	pBJ114 Δ(*sinKM*) Km^r	This study
pET32a	Trx-His overexpression vector, Ap^r	Novagen
pMG022	pET32a *sinK* Ap^r	This study
pMG023	pET32a $sinK_{H45A}$ Ap^r	This study

[a]Km^r, kanamycin resistant; RNAP, RNA polymerase; Ap^r, apramycin resistant.

For analysis of 96-well submerged cultures, each strain was seeded into 5 wells and induced to develop as described above. After 24 h of development (T = 24), plates were placed in a Tecan Spark M10 plate reader (preheated to 32°C), and the center of each well was imaged every 30 min for the next 48 h (T = 24 to 72 h development). The resulting images were assembled with ImageJ (43). For each movie generated, the frame in which aggregation was first observed was recorded and the time of development was calculated. Maximum aggregates were enumerated from the single frame in which the most aggregation centers were observed. Final fruiting bodies were enumerated from the last frame recorded (at T = 72 h). Data were compiled from three independent biological experiments, each with 5 replicates per strain. Aggregate mobility was calculated as $[(Agg_{mf} - Agg_{mi}) \times 0.5$ h/frame], where Agg_{mi} was the first frame in which fully formed aggregates made net *x*/*y* displacement, and Agg_{mf} was the first frame in which aggregates made no net *x*/*y* displacement. Average aggregate mobility was calculated from at least two replicates in two independent biological experiments.

Sporulation assays. To determine the number of spores produced, cells were induced to develop under submerged culture in 24-well tissue culture plates. For each time point, triplicate samples of developing cells were harvested from wells and pelleted for 5 min at 13,000 × *g*, and the supernatant was removed and stored at −20°C until further use. Pellets were resuspended in 0.5 ml of sterile water, heated at 50°C for 60 min, and sonicated at 30% output for 15 s (0.5-s pulses) using a microtip and Branson Sonifier 250 (Branson Ultrasonics). Phase-bright spores were counted with a Helber bacteria counting chamber (Hawksley, UK) and reported as the average and associated standard deviation of the total spores per 24-well culture.

Quantitative real-time PCR. *sinK* mRNA levels were examined using quantitative real-time reverse transcriptase PCR. The wild-type strain DZ2 was developed under submerged culture in 100-mm petri dishes as described above. Total RNA was isolated using the hot phenol method (44), treated with RNase-free DNase I (Fermentas), and transcribed into cDNA using random hexamer primers (Amersham) and SuperScript III reverse transcriptase (Invitrogen), as described previously in detail (44). Real-time PCR was performed in a 7300 real-time PCR system (Applied Biosystems) using SYBR green PCR master mix (Applied Biosystems), *sinK* primers (oPH1432/oPH1433), and 2 μl of 1:20 dilutions of cDNA reaction mixtures in 26-μl total reactions for each time point in duplicate. Control reactions using mock cDNA reaction mixtures (reverse transcriptase omitted) or 10, 1, 0.1, or 0.01 ng genomic DNA were also performed. The real-time PCR cycle conditions were as follows: 50°C for 2 min, 95°C for 10 min, and 40 cycles of 95°C for 15 s and 60°C for 1 min. Melting and dissociation curves were determined using 95°C for 15 s, 60°C for 30 s, and 95°C for 15 s; single peaks were verified for each sample. Threshold cycle (C_T)

values for each reaction were assigned automatically by the system software (7300 System SDS software version 1.2.3). Average C_T values were calculated from two technical replicates. *sinK* primer efficiency of 1.906 was calculated from a standard curve of genomic DNA. The relative fold induction of *sinK* was determined as $1.906^{-(CT\ \text{sample}\ -\ CT\ \text{T=0})}$, and the average fold induction from two replicate experiments versus time of development was plotted.

Overexpression and purification of recombinant protein. pET32a plasmids carrying $sinK_{WT}$ (pMG022) or $sinK_{H45A}$ (pMG023) were expressed in the salt-inducible *E. coli* strain GJ1158 (45). Cultures were grown with shaking (220 rpm) to early mid-logarithmic phase (optical density at 600 nm [OD_{600}], 0.5) at 37°C, transferred to 18°C, and further incubated until late-mid-logarithmic phase (OD_{600}, 0.7). To induce recombinant proteins, 300 mM NaCl (final concentration) was added, and cells were further incubated overnight at 18°C. Cultures were harvested and stored at −20°C. We could detect no insoluble Trx-SinK produced under these conditions.

Cell pellets were resuspended in binding buffer (50 mM Tris [pH 7.6], 300 mM NaCl, 20 mM imidazole), supplemented with 1:150 mammalian protease inhibitor cocktail (Sigma), and disrupted by French press (18,000 lb/in^2) in three cycles. Lysates were cleared first by centrifugation at 3,500 × *g* for 15 min 4°C and again by centrifugation at 20,000 × *g* for 30 min at 4°C. Trx-His_6-SinK proteins were purified using a fast protein liquid chromatography (FPLC) affinity system (Äkta Technology, GE Healthcare) using a 1-ml HisFF1 trap nickel affinity column (GE Healthcare) with a flow rate of 1 ml/min at 4°C. The column was washed with 15 to 25 column volumes (CV) of binding buffer, and elution was performed by a gradient of 20 to 500 mM imidazole supplemented to the binding buffer. One-milliliter fractions were collected and resolved by SDS-PAGE, and fractions containing peak Trx-His_6-SinK proteins were pooled and dialyzed overnight at 4°C against storage buffer (50 mM Tris [pH 8], 10% [vol/vol] glycerol, 150 mM NaCl, 1 mM dithiothreitol [DTT]).

***In vitro* phosphorylation and phosphor stability assays.** For *in vitro* phosphorylation assays, 10 μM purified protein in phosphorylation reaction buffer (storage buffer supplemented with 5 mM $MgCl_2$, 50 mM KCl) was incubated with 0.5 mM ATP and 1.7 μM [γ-^{32}P]ATP (222 TBq/mmol; Hartmann Analytic, Braunschweig, Germany) for 0 to 60 min at 32°C. For each time point, a 10-μl sample was quenched with an equal volume of 2× LSB (125 mM Tris-HCl, 20% [vol/vol] glycerol, 4% [wt/vol] SDS, 10% β-mercaptoethanol, 0.02% [wt/vol] bromophenol blue) and immediately frozen at –20°C. Samples were resolved by SDS-PAGE (12% acrylamide gels), exposed to a storage phosphor screen (GE Healthcare) overnight, and analyzed using a Storm 800 imaging system (GE Healthcare). Gels were subsequently stained with Coomassie blue dye.

To test the chemical stability of phosphor groups on SinK, an autophosphorylation reaction was performed for 60 min and quenched as described above, and 20-μl aliquots were either frozen immediately at –20°C or treated with 4 μl of 1 M NaOH, 1 M HCl, or H_2O, and incubated for 1 h at 42°C (30). The reactions were resolved, and ^{32}P-labeled SinK was detected as described above. Signal intensities were quantified using ImageJ 1.43u and plotted using Excel. Gels were subsequently stained using Coomassie blue dye.

Generation of anti-SinK immunosera. Rabbit anti-SinK antibodies were generated by Eurogentec (Belgium) using a 28-day immunization program. Anti-SinK antibodies were affinity purified from immune serum using purified Trx-His_6-SinK. Briefly, 2 ml serum was purified against 1 mg Trx-His_6-SinK resolved by SDS-PAGE and transferred to a polyvinylidene difluoride (PVDF) membrane. The membrane was stained with 0.1% (wt/vol) Ponceau S and 5% acetic acid, and the Trx-His_6-SinK strip of membrane was cut out, destained with water, washed with glycine buffer (100 mM glycine [pH 2.5]), washed twice with TBS-T (20 mM Tris [pH 7.4], 500 mM NaCl, 0.05% [vol/vol] Tween 20), and blocked in 3% (wt/vol) bovine serum albumin (BSA) in TBS-T for 2 h at room temperature (RT) with rotation. Two milliliters of serum in 8 ml TBS-T was incubated with the PVDF strip overnight at 4°C. The strip was then washed once in TBS-T for 2 min and twice with phosphate-buffered saline (PBS) for 5 min. To elute anti-SinK-specific antibodies, 1 ml of glycine buffer was added for 10 min, and the supernatant was immediately neutralized with 125 μl of 1 M Tris (pH 8.0). BSA and sodium azide were added to 1 mg ml^{-1} and 0.002%, respectively, and aliquots were stored at −20°C.

Cell lysate preparation and immunoblot analysis. For immunoblotting of developing cell lysates, *M. xanthus* strains were developed in 100-mm petri dishes, as described above. At the indicated time points, cells were harvested, pelleted at 4,696 × *g* and 4°C for 10 min, resuspended in 400 μl MMC-PI (MMC containing 1:20 dilution mammalian protease inhibitor cocktail; Sigma), and disrupted by beating with 0.1-mm zirconium beads six times for 45 s at 6.5 m s^{-1} at 4°C. Protein concentration was determined using a bicinchoninic acid (BCA) assay (Pierce), and samples were prepared to 2 μg μl^{-1} in 2× LSB and heated at 99°C for 5 min. Ten micrograms of each sample was resolved by denaturing SDS-PAGE on 8% polyacrylamide (29:1) gels and transferred to PVDF membranes using a semidry transfer apparatus (Hoefer). Western blot analyses were performed using affinity-purified anti-SinK primary antibodies at a 1:100 dilution probed overnight at 4°C. Goat anti-rabbit IgG secondary antibodies conjugated to horseradish peroxidase (HRP; Pierce) were used at a dilution of 1:20,000, and signal was detected with enhanced chemiluminescence substrate (Thermo Fisher Scientific), followed by exposure to autoradiography film (Kodak).

Operon analysis. cDNA was generated by reverse transcription of mRNA isolated from *M. xanthus* DZ2 cells induced to develop under submerged culture for 3 h as described above, except reverse primer oPH1025 specific to MXAN_4466 was used. A mock reaction in which reverse transcriptase was replaced with water was also performed. PCRs using 2 μl of a 1:20 dilution cDNA reaction or mock reaction mixture, or 200 ng genomic DNA as the template and primers specific to internal *sinK* (oPH996/oPH997)

fragments, internal *sinM* (oPH1027/oPH1028) fragments, or the *sinK-sinM* junction (oPH1026/oPH1028) were performed as described previously (44).

SUPPLEMENTAL MATERIAL

Supplemental material for this article may be found at https://doi.org/10.1128/JB.00561-18.

SUPPLEMENTAL FILE 1, PDF file, 1.1 MB.
SUPPLEMENTAL FILE 2, AVI file, 2.3 MB.
SUPPLEMENTAL FILE 3, AVI file, 2.1 MB.
SUPPLEMENTAL FILE 4, AVI file, 2.1 MB.
SUPPLEMENTAL FILE 5, AVI file, 2.7 MB.
SUPPLEMENTAL FILE 6, AVI file, 2.1 MB.
SUPPLEMENTAL FILE 7, AVI file, 2.2 MB.
SUPPLEMENTAL FILE 8, AVI file, 2.2 MB.

ACKNOWLEDGMENTS

We gratefully acknowledge Patrick McLaughlin for his input in the high-resolution submerged-culture assays, Roy Welch and Fatmagul Bahar (Syracuse University) for discussions on video microscopy, Bongsoo Lee for generating strain PH2000, Lotte Sogaard-Andersen (MPI-Terrestrial Microbiology) for hosting Maike Glaser during her data analysis stage, and members of the Higgs lab for critical comments on the manuscript.

Funding was provided by the National Science Foundation (grant IOS-1651921) (to P.I.H.), Wayne State University start-up funds, the Max Planck Society, and the International Max Planck Research School for Environmental, Cellular and Molecular Microbiology (M.M.G.).

REFERENCES

1. Galperin MY. 2005. A census of membrane-bound and intracellular signal transduction proteins in bacteria: bacterial IQ, extroverts and introverts. BMC Microbiol 5:35. https://doi.org/10.1186/1471-2180-5-35.
2. Ulrich LE, Zhulin IB. 2010. The MiST2 database: a comprehensive genomics resource on microbial signal transduction. Nucleic Acids Res 38:D401–D407. https://doi.org/10.1093/nar/gkp940.
3. Stock AM, Robinson VL, Goudreau PN. 2000. Two-component signal transduction. Annu Rev Biochem 69:183–215. https://doi.org/10.1146/annurev.biochem.69.1.183.
4. Galperin MY. 2006. Structural classification of bacterial response regulators: diversity of output domains and domain combinations. J Bacteriol 188:4169–4182. https://doi.org/10.1128/JB.01887-05.
5. Bourret RB. 2010. Receiver domain structure and function in response regulator proteins. Curr Opin Microbiol 13:142–149. https://doi.org/10.1016/j.mib.2010.01.015.
6. Whitworth DE, Cock PJ. 2009. Evolution of prokaryotic two-component systems: insights from comparative genomics. Amino Acids 37:459–466. https://doi.org/10.1007/s00726-009-0259-2.
7. Capra EJ, Laub MT. 2012. Evolution of two-component signal transduction systems. Annu Rev Microbiol 66:325–347. https://doi.org/10.1146/annurev-micro-092611-150039.
8. Mascher T, Helmann JD, Unden G. 2006. Stimulus perception in bacterial signal-transducing histidine kinases. Microbiol Mol Biol Rev 70:910–938. https://doi.org/10.1128/MMBR.00020-06.
9. Jung K, Fried L, Behr S, Heermann R. 2012. Histidine kinases and response regulators in networks. Curr Opin Microbiol 15:118–124. https://doi.org/10.1016/j.mib.2011.11.009.
10. Muñoz-Dorado J, Marcos-Torres FJ, García-Bravo E, Moraleda-Muñoz A, Pérez J. 2016. Myxobacteria: moving, killing, feeding, and surviving together. Front Microbiol 7:781. https://doi.org/10.3389/fmicb.2016.00781.
11. O'Connor KA, Zusman DR. 1991. Development in *Myxococcus xanthus* involves differentiation into two cell types, peripheral rods and spores. J Bacteriol 173:3318–3333. https://doi.org/10.1128/jb.173.11.3318-3333.1991.
12. Costerton JW, Cheng KJ, Geesey GG, Ladd TI, Nickel JC, Dasgupta M, Marrie TJ. 1987. Bacterial biofilms in nature and disease. Annu Rev Microbiol 41:435–464. https://doi.org/10.1146/annurev.mi.41.100187.002251.
13. Flemming HC, Wingender J, Szewzyk U, Steinberg P, Rice SA, Kjelleberg S. 2016. Biofilms: an emergent form of bacterial life. Nat Rev Microbiol 14:563–575. https://doi.org/10.1038/nrmicro.2016.94.
14. Hu W, Lux R, Shi W. 2013. Analysis of exopolysaccharides in Myxococcus xanthus using confocal laser scanning microscopy. Methods Mol Biol 966:121–131. https://doi.org/10.1007/978-1-62703-245-2_8.
15. Higgs PI, Hartzell P, Holkenbrink C, Hoiczyk E. 2014. Myxococcus xanthus vegetative and developmental cell heterogeneity, p 51–77. *In* Yang Z, Higgs PI (ed), Myxobacteria: genomics and molecular biology. Caister Academic Press, Norfolk, United Kingdom.
16. Lee B, Holkenbrink C, Treuner-Lange A, Higgs PI. 2012. *Myxococcus xanthus* developmental cell fate production: heterogeneous accumulation of developmental regulatory proteins and reexamination of the role of MazF in developmental lysis. J Bacteriol 194:3058–3068. https://doi.org/10.1128/JB.06756-11.
17. Goldman B, Bhat S, Shimkets LJ. 2007. Genome evolution and the emergence of fruiting body development in *Myxococcus xanthus*. PLoS One 2:e1329. https://doi.org/10.1371/journal.pone.0001329.
18. Whitworth DE, Cock PJ. 2008. Two-component systems of the myxobacteria: structure, diversity and evolutionary relationships. Microbiology 154:360–372. https://doi.org/10.1099/mic.0.2007/013672-0.
19. Shi X, Wegener-Feldbrügge S, Huntley S, Hamann N, Hedderich R, Søgaard-Andersen L. 2008. Bioinformatics and experimental analysis of proteins of two-component systems in *Myxococcus xanthus*. J Bacteriol 190:613–624. https://doi.org/10.1128/JB.01502-07.
20. Muñoz-Dorado J, Higgs PI, Elias-Arnanz M. 2014. Abundance and complexity of signaling mechanisms in the myxobacteria, p 127–149. *In* Yang Z, Higgs PI (ed), Myxobacteria: genomics and molecular biology. Caister Academic Press, Norfolk, United Kingdom.
21. Pérez J, Castañeda-García A, Jenke-Kodama H, Müller R, Muñoz-Dorado J. 2008. Eukaryotic-like protein kinases in the prokaryotes and the myxobacterial kinome. Proc Natl Acad Sci U S A 105:15950–15955. https://doi.org/10.1073/pnas.0806851105.
22. Wegener-Feldbrugge S, Sogaard-Andersen L. 2009. The atypical hybrid histidine protein kinase RodK in *Myxococcus xanthus*: spatial proximity supersedes kinetic preference in phosphotransfer reactions. J Bacteriol 191:1765–1776. https://doi.org/10.1128/JB.01405-08.
23. Jagadeesan S, Mann P, Schink CW, Higgs PI. 2009. A novel "four-

component" two-component signal transduction mechanism regulates developmental progression in *Myxococcus xanthus*. J Biol Chem 284:21435–21445. https://doi.org/10.1074/jbc.M109.033415.
24. Willett JW, Kirby JR. 2011. CrdS and CrdA comprise a two-component system that is cooperatively regulated by the Che3 chemosensory system in *Myxococcus xanthus*. mBio 2:e00110-11. https://doi.org/10.11128/mBio.00110-11.
25. Schramm A, Lee B, Higgs PI. 2012. Intra- and interprotein phosphorylation between two-hybrid histidine kinases controls *Myxococcus xanthus* developmental progression. J Biol Chem 287:25060–25072. https://doi.org/10.1074/jbc.M112.387241.
26. Bretl DJ, Muller S, Ladd KM, Atkinson SN, Kirby JR. 2016. Type IV-pili dependent motility is co-regulated by PilSR and PilS2R2 two-component systems via distinct pathways in Myxococcus xanthus. Mol Microbiol 102:37–53. https://doi.org/10.1111/mmi.13445.
27. Wu SS, Kaiser D. 1997. Regulation of expression of the *pilA* gene in *Myxococcus xanthus*. J Bacteriol 179:7748–7758.
28. Letunic I, Doerks T, Bork P. 2009. SMART 6: recent updates and new developments. Nucleic Acids Res 37:D229–D232. https://doi.org/10.1093/nar/gkn808.
29. Letunic I, Copley RR, Pils B, Pinkert S, Schultz J, Bork P. 2006. SMART 5: domains in the context of genomes and networks. Nucleic Acids Res 34:D257–D260. https://doi.org/10.1093/nar/gkj079.
30. Duclos B, Marcandier S, Cozzone AJ. 1991. Chemical properties and separation of phosphoamino acids by thin-layer chromatography and/or electrophoresis. Methods Enzymol 201:10–21.
31. Robinson M, Son B, Kroos D, Kroos L. 2014. Transcription factor MrpC binds to promoter regions of hundreds of developmentally-regulated genes in *Myxococcus xanthus*. BMC Genomics 15:1123. https://doi.org/10.1186/1471-2164-15-1123.
32. McLaughlin PT, Bhardwaj V, Feeley BE, Higgs PI. 2018. MrpC, a CRP/Fnr homolog, functions as a negative autoregulator during the *Myxococcus xanthus* multicellular developmental program. Mol Microbiol 109:245–261. https://doi.org/10.1111/mmi.13982.
33. Müller FD, Schink CW, Hoiczyk E, Cserti E, Higgs PI. 2012. Spore formation in *Myxococcus xanthus* is tied to cytoskeleton functions and polysaccharide spore coat deposition. Mol Microbiol 83:486–505. https://doi.org/10.1111/j.1365-2958.2011.07944.x.
34. Rasmussen AA, Wegener-Feldbrügge S, Porter SL, Armitage JP, Søgaard-Andersen L. 2006. Four signalling domains in the hybrid histidine protein kinase RodK of *Myxococcus xanthus* are required for activity. Mol Microbiol 60:525–534. https://doi.org/10.1111/j.1365-2958.2006.05118.x.
35. Cho K, Zusman DR. 1999. Sporulation timing in *Myxococcus xanthus* is controlled by the *espAB* locus. Mol Microbiol 34:714–725.
36. Guzzo M, Murray SM, Martineau E, Lhospice S, Baronian G, My L, Zhang Y, Espinosa L, Vincentelli R, Bratton BP, Shaevitz JW, Molle V, Howard M, Mignot T. 2018. A gated relaxation oscillator mediated by FrzX controls morphogenetic movements in Myxococcus xanthus. Nat Microbiol 3:948–959. https://doi.org/10.1038/s41564-018-0203-x.
37. Borland S, Prigent-Combaret C, Wisniewski-Dyé F. 2016. Bacterial hybrid histidine kinases in plant-bacteria interactions. Microbiology 162:1715–1734. https://doi.org/10.1099/mic.0.000370.
38. Maniatis T, Fritsch EF, Sambrook J. 1982. Molecular cloning: a laboratory manual. Cold Spring Harbor Laboratory Press, Cold Spring Harbor, NY.
39. Campos JM, Zusman DR. 1975. Regulation of development in *Myxococcus xanthus*: effect of 3′:5′-cyclic AMP, ADP, and nutrition. Proc Natl Acad Sci U S A 72:518–522.
40. Lee B, Schramm A, Jagadeesan S, Higgs PI. 2010. Two-component systems and regulation of developmental progression in *Myxococcus xanthus*. Methods Enzymol 471:253–278. https://doi.org/10.1016/S0076-6879(10)71014-4.
41. Ueki T, Inouye S, Inouye M. 1996. Positive-negative KG cassettes for construction of multi-gene deletions using a single drug marker. Gene 183:153–157.
42. Magrini V, Creighton C, Youderian P. 1999. Site-specific recombination of temperate *Myxococcus xanthus* phage Mx8: genetic elements required for integration. J Bacteriol 181:4050–4061.
43. Abramoff MD, Magalhaes PJ, Ram SJ. 2004. Image processing with ImageJ. Biophotonics Int 11:7.
44. Müller FD, Treuner-Lange A, Heider J, Huntley SM, Higgs PI. 2010. Global transcriptome analysis of spore formation in *Myxococcus xanthus* reveals a locus necessary for cell differentiation. BMC Genomics 11:264. https://doi.org/10.1186/1471-2164-11-264.
45. Bhandari P, Gowrishankar J. 1997. An *Escherichia coli* host strain useful for efficient overproduction of cloned gene products with NaCl as the inducer. J Bacteriol 179:4403–4406.
46. Schultz J, Milpetz F, Bork P, Ponting CP. 1998. SMART, a simple modular architecture research tool: identification of signaling domains. Proc Natl Acad Sci U S A 95:5857–5864.
47. Julien B, Kaiser AD, Garza A. 2000. Spatial control of cell differentiation in *Myxococcus xanthus*. Proc Natl Acad Sci U S A 97:9098–9103.
48. Wu SS, Kaiser D. 1996. Markerless deletions of *pil* genes in *Myxococcus xanthus* generated by counterselection with the *Bacillus subtilis sacB* gene. J Bacteriol 178:5817–5821. https://doi.org/10.1128/jb.178.19.5817-5821.1996.